# A Newtonian Alternative To Special Relativity

By:
Eric A Samuel
*George Mason University*

## *Abstract*

This paper offers elegant Newtonian explanations for key experiments that support special relativity (SR).  Rossi's high altitude μ-meson measurements are shown to accurately reveal μ-meson flight times between known altitudes, consistent with μ-meson speeds of up to 20 c, thus contradicting SR's universal speed limit concept.  The speed-limited E-field and spiral H-field trajectories of electrons are explained classically by augmenting the Lorentz force with a flux-proportional radiation damping Lentz force:

$$F = \left( e\,\vec{E} + e\,\vec{v} \times \vec{B} \right) - \left[ \frac{e}{c} (\vec{v} \cdot \vec{E}) \frac{\vec{E}}{|\vec{E}|} \; + \; e\,\alpha \frac{\vec{B} \times \vec{v} \times \vec{B}}{|\vec{B}|} \right]$$

In the above model, an electron in an E-field reaches a terminal velocity of c when its Lorentz motive and radiation damping forces are equally opposed. The spiral trajectories of charged particles in H-fields are shown to be due to the progressive radiation dampening of their tangential velocities while their Lawrence cyclotron frequencies remain unaffected.  The remarkable experiments of Ives and Stillwell, and of Kundig are re-interpreted as being due to impulsive momentum transfer to photons emitted from accelerating molecules or nuclei. However, the impulsive momentum transfer time is a fraction of the photon emitter lifetime that is proportional to the characteristic light transit time.

SR's time-dilatation formulation is shown to be theoretically flawed because: (i) both its postulates are traceable to Newton's *Corollary V*, in which time and mass invariance are implicit, and (ii) SR's unjustified expectation of an inertial frame outcome for a non-inertial experimental design that places observer and apparatus in separate frames; a simple solution by Galilean velocity transformation proves no time dilation. Additionally, SR's time dilation formulation is ambiguous for rotations and wave-clock types.  Replacing the light clock with a sonar clock also leads to ambiguous time dilations and an unlikely upper speed limit.

Consequently, Newton's laws alone are sufficient to fully explain the experimental data that are now believed to support SR.

# Introduction

This paper arose from a compelling need to re-examine the fundamental basis of special relativity (SR) because of SR's unjustified dismissal of the applicability of Newton's laws in the realm of fundamental particle kinematics. Newton originally defined inertial frames of reference in Corollary V (C5) of Principia (1): *The motions of bodies included in a given space are the same among themselves, whether that space is at rest, or moves uniformly forwards in a right line without any circular motion. A clear proof of which we have the experiment of a ship, where all motions happen after the same manner whether the ship is at rest or is carried forward in a right line.*

The invariance of time and mass across inertial frames is implicit in C5. The fundamental physical constants, such as the speed of light and Planck's constant, are also invariant, because they are the same inertial frame outcomes of duplicate experiments designed to measure them. Accordingly, measurements from identical experiments in inertial frames moving at different speeds will be identical (within experimental error); consequently, the speeds of inertial frames are unknowable from experimental measurements within them. The above expectation is fully borne out in the modern experimental record of experimental reproducibility in laboratories at different latitudes around the world that have different surface velocities due to Earth's rotation (accounting for the small fictitious accelerations introduced from Earth's rotational centripetal acceleration). The above complying inertial frame experience includes, most importantly, the invariance of time at various latitudes as measured by highly precise atomic clocks, a dozen or more of which are deployed on Earth.

SR is purportedly built on two postulates; its first postulate is identical to Newton's C5. SR's second postulate is redundant, because the modern experimental record verifies that the fundamental physical constants, of which c, the speed of light is one, are preserved across inertial frames. Hence SR is built only on C5. Two emerging logical conjectures are: (1) SR, although emanating from C5, comes to a different and radical conclusion of an observed time dilation and mass variance, other than C5's implied time and mass invariance, and (2) SR's time dilation and mass variance conclusion directly contradict its C5 starting postulate. Resolving the above conjectures is the main purpose of the present study; the study is further justified by the following troubling concerns about SR's theoretical viability:

(1) SR's total energy formulation that assigns large energy total energy changes to particles having infinitesimal changes in velocity violates the kinetic energy theorem which states that the kinetic energy change is the indicator of the total work done on the particle. Furthermore, SR's total energy cannot qualify as a state variable because it is not measurable but is only derived from measurable kinetic energy.

(2) Despite its universal acceptance, SR has been exempted from simple rigorousness checks, such as invariance with respect to rotations, and invariance with respect to different wave clocks, such as sonar clocks.

(3) There appears to be a predisposition to SR in the data analyses of the many remarkable experiments believed to support SR; they show experimental data agreement with SR only, but often lack conscious, thoughtful deliberations of potential reasons for the inapplicability of Newtonian laws.

(4) The above surety in SR has led to poor data analysis practices. The speeds of fundamental particles were not carefully measured to verify SR's universal speed limit. Instead, experimental data, such as bubble chamber tracks or upper atmospheric μ-meson data, have been preconditioned as if tacitly obeying the universal speed limit.

(5) SR does not provide an explanation for the spiral trajectories of charged particles in magnetic fields.

(6) The arrival of μ-mesons on Earth is often quoted as a successful application of time dilation. However, time dilation is not at all necessary to explain the measured concentrations of μ-mesons on the earth's surface because, the half-life of the μ- meson decay merely characterizes the exponential distribution of the actual decay times. Clearly there will always be a concentration of μ-mesons that arrive on Earth whose actual decay times are longer that their times of flight from their origins in space.

It appears that the experimental literature is overwhelmingly lacking in challenging SR with alternative explanations for the experiments that are currently interpreted as exclusively favoring SR.

The main breakthrough theme pervading the present study is that Newtonian laws alone are sufficient to explain every experimental support claimed for SR, without the complexity of time and mass variance, and without the above-listed controversies.

The Results section of the paper is organized into four subsections for exemplifying the unifying theme:

(1) Experimental measurements of the speeds of upper-atmospheric μ-mesons provide evidence against SR's universal speed limit

(2) Newtonian explanations of the experimentally observed electron trajectories in electric and magnetic fields using a simple force model for radiation damping to augment the Lorentz force on the electron

(3) a classical explanation for experiments apparently confirming SR's transverse Doppler effect with a newly proposed phenomenon of impulsive momentum transfer to photons emitted from accelerated ions or nuclei

(4) A critical analysis of SR's time dilation derivation and its resolution by means of a Galilean velocity transformation.

The discussions are focused on restoring the applicability of Newton's laws alone to solve the kinematics of fundamental particles and thus to obviate the currently accepted complications of time and mass non-invariance across inertial frames. The paper concludes with a discourse of the implications of Newtonian restoration.

## Method

The method used in this study is mindful that physics is an experimental science and that new concepts need to be validated against experimental data, while also being consistent with previously established principles. Only Newton's laws of motion, and datasets that are available in curated publications, are used to test the new concepts advanced in this study. The speeds of μ-meson speeds presented in the study were obtained by careful analysis of experimental data to extract μ-meson flight times between known altitudes, and from published measurements of the mean distance travelled in the meson's half-life time. The new explanations for the kinematics of charged particles exposed to electromagnetic fields presented in this study arose first from identifying the radiation damping as a missing viable force, modeling that radiation damping force (RDF) as a Lentz force, and finally testing the modeled RDF against published datasets. The impulsive momentum transfer concept presented in this study is an application of a quintessential Newtonian concept, that is borne out by published experimental data.

# Results

## 1.  μ-meson Flight Speeds

## 1.1  Flight Speeds From Decay-Time Distributions

Rossi *et al.* (3, 4, 5) performed three types of μ-meson flight experiments that are amenable to analyses of the μ-meson flight speeds: (i) decay time distribution profiles by altitude (3), (ii) μ-meson total count by altitude (4), and (iii) μ-meson decay rate by altitude (5).

Rossi, Sands, and Sard (3) performed a remarkable experiment to measure the μ-meson decay profiles in Chicago, Denver, Echo Lake, and Mt. Evans which, as shown in Figure 1, vary significantly by altitude. The above altitude-dependent decay distributions can be analyzed for accurate estimates of meson travel times across altitudes, as follows.  Consider mesons travelling between two altitudes, A and B.  The decay time distribution at the reference altitude, $A$, is:

$$N = N_A \, e^{-\frac{t}{\tau}}, \qquad 0 \leq t < \infty \qquad\qquad -(1)-$$

where $N_A$ is the reference meson count and $\tau$ is the meson half-life. Because, by definition, the meson population at altitude, B, will not contain any mesons with lifetimes $< t_1$, the mean meson travel time between those altitudes, A and B, the decay time distribution at the lower altitude, $B$, referenced to the clock at A is given by Equation (2) which is the same as Equation (1), but with zero counts below $t < t_1$:

$$N = 0, \qquad\quad t < t_1, \quad and$$

$$N = N_A \, e^{-\frac{t}{\tau}}, \qquad t_1 \leq t < \infty \qquad\qquad -(2)-$$

Because the population distribution arriving at altitude B, is depleted of decay times $t < t_1$, the *local* decay time distribution referenced to the clock at B, is:

$$N = N_B \, e^{-\frac{t}{\tau}}, \qquad N_B = N_A \, e^{-\frac{t_1}{\tau}} \qquad\qquad -(3)-$$

where $N_B$ is the total depleted count at B.  Combining both Equations (3) above, the local decay time distribution at B, is:

$$N = N_A \, e^{-\frac{(t_1+t)}{\tau}} = \left(N_A \, e^{-\frac{t_1}{\tau}}\right) e^{-\frac{t}{\tau}} \qquad\qquad -(4)-$$

Equation (4) shows that the local decay time distribution at B can be interpreted alternately as the local decay time distribution at A, time shifted to the left by the flight time, $t_1$.

Figure 1 illustrates the flight-depleted decay time distribution variations as discussed above, in which a population of fictitious particles with a decay half-life of 2 $\mu$sec, and whose decay profiles were measured by four coincidence timers set at 0.5, 1.0, 1.5 and 2.0 $\mu$sec at two locations, A and B, of different altitudes, the second, lower location (Location B) being chosen for a flight time, $\Delta\tau = 3$ $\mu$sec from the upper A location.
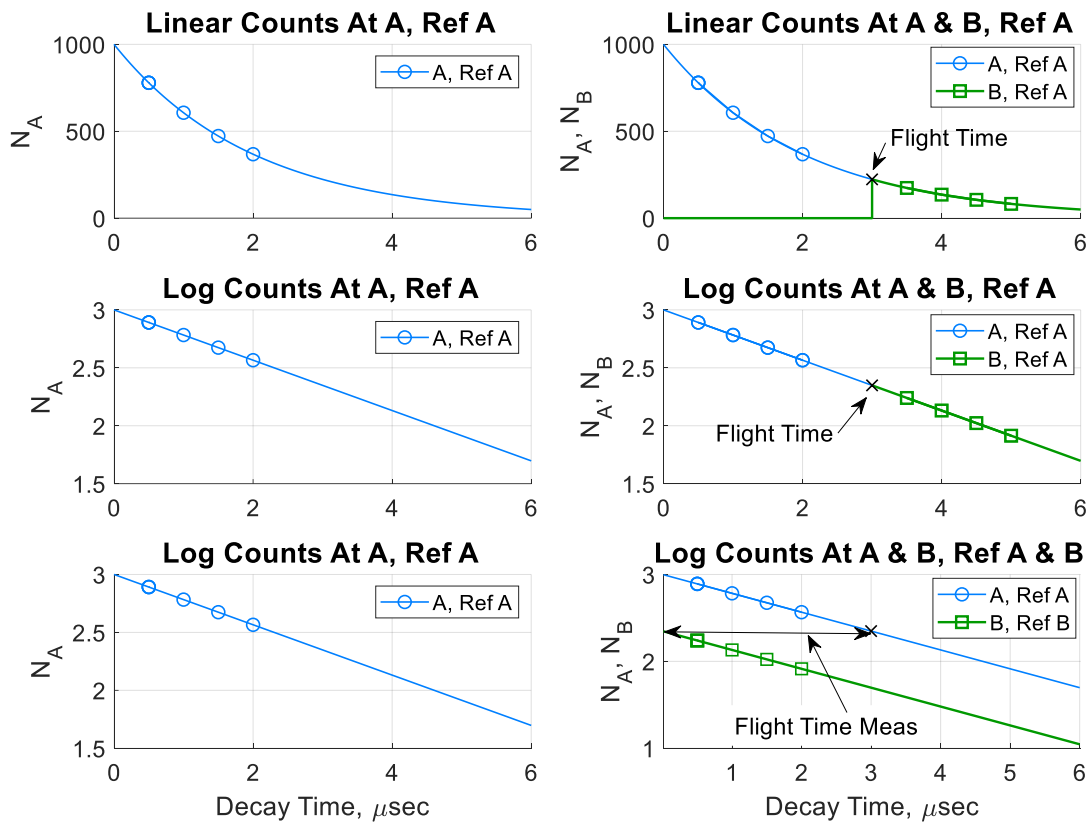


**Figure 1.** *Illustration of the decay-time distributions given by Equations 1-4, for a fictitious particle with a half-life of 2 $\mu$sec. at 2 altitudes, A and B, separated by a flight time of 3 $\mu$sec. The time shift measurement interpretation is indicated in the Figure's lowest right panel.*

The decay time distributions measured by Rossi *et al.* (3) are shown in Figure 2, in which the horizontal intercepts between successive altitudes are clearly identified.
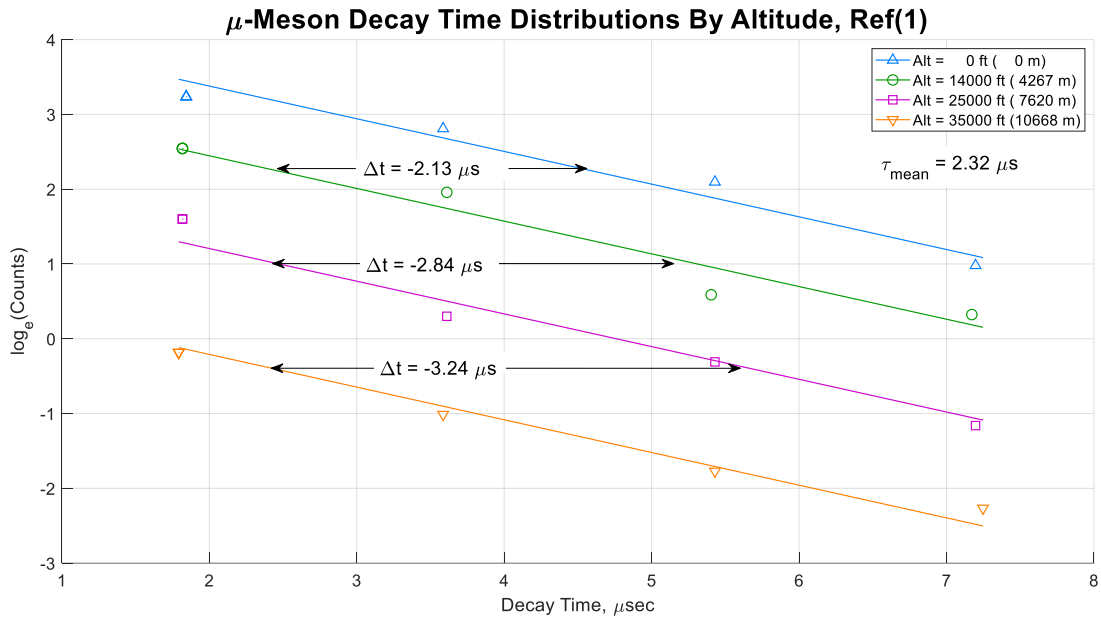
**Figure 2.** *Decay time distributions measured by Rossi, Sands, and Sard (3) in which the flight time between successive altitudes are identified.*

**Table 1**. *μ-Meson flight time and flight speed estimation from decay time distribution measurements.*

| Altitude, z | | | | | | |
|---|---|---|---|---|---|---|
| ft | m | $\Delta z$ m | Time Intercept, μs | $\Delta t$ (Flight Time), μs | Flight Speed, v, m/s | Warp Num |
| 35,000 | 10,668 | | 9.73 | | | |
| 25,000 | 7,620 | 3,048 | 7.60 | 2.13 | 1.43E+09 | 4.8 |
| 14,000 | 4,267 | 3,353 | 4.76 | 2.84 | 1.18E+09 | 3.9 |
| 0 | 0 | 4,267 | 1.52 | 3.24 | 1.32E+09 | 4.4 |

Table 1 provides simple calculations for the mean μ-meson flight speeds between altitudes and reveals that $\mu$-mesons consistently exceed the speed of light, c.

## 1.2 Flight Speeds From Total Counts and From Decay-Rates

Rossi and Hall's (4) measurements of the total meson count rate variation with altitude, can also be interpreted in terms of the characteristic decay distances, $\lambda_\sigma$ or $\lambda_z$, the mean meson flight distances in $\sigma$-space or in altitude (z-space) within a decay half-life. Rossi showed that the total meson count rate, N, decays exponentially in air with respect to $\sigma$, the density-corrected altitude, as follows:

$$N = N_0 e^{-\frac{\sigma}{\lambda_\sigma}}, \qquad \sigma = \rho z \qquad\qquad -(5)-$$

where $\rho$ is the air density at altitude z, and the mean distances between decays, $\lambda_\sigma$ and $\lambda_z$ are related by:

$$\lambda_z = \lambda_\sigma \frac{dz}{d\sigma} \qquad\qquad -(6)-$$

Rossi and Hall measured the μ-meson count rate at close to sea level in Chicago, and at Echo Lake, Co, which is at an elevation of approximately 2 miles. Rossi *et al.* (5) measured the μ-meson decay rate on Mt. Evans, Echo Lake, and in Denver, and Chicago. Both sets of authors report mean $\lambda_z$ values derived from their measurements, as shown in Table 2, in which the mean flight speeds, v, are derived from the reported $\lambda_z$ values, as follows:

$$v = \frac{\lambda_z}{\tau}, \qquad \tau = 2.2\text{x}10^{-6} \qquad\qquad -(7)-$$

$\tau$ being the mean half-life of $\mu$-mesons.

**Table 2.** *μ-meson flight speed estimation from total μ-meson count rate and total μ-meson decay rate measurements.*

| Location | Altitude, z, m | $\sigma, \frac{g}{cm^2}$ | $\lambda_z$, km | Flight Speed, v, m/s | Warp No | Ref-erence |
|---|---|---|---|---|---|---|
| Echo Lake | 3240 | 709 | 13.3 | 6.05E+09 | 20.2 | 4 |
| Denver | 1616 | 856 | 4.5 | 2.05E+09 | 6.8 | 4 |
| | | | | | | |
| Mt. Evans | 4348 | 616-700 | 9.4 | 4.27E+09 | 14.2 | 5 |
| Echo Lake | 3240 | 699-786 | 9.9 | 4.50E+09 | 15.0 | 5 |
| Denver | 1616 | 857-944 | 9.5 | 4.32E+09 | 14.4 | 5 |
| Chicago | 180 | 1010 | 9.4 | 4.27E+09 | 14.2 | 5 |

The μ-meson flight speeds estimated from the mean distance to decay, $\lambda_z$, derived from the meson count rate or the meson decay rate are also seen to be excessively higher than the speed of light.

## 2. Electron Motion in Magnetic and Electric Fields

### 2.1 Electron Motion in Magnetic Fields

It is well known from the bubble chamber images that the trajectories of electrons, positrons and other charged particles are inward looping spirals whose spiraling directions, clockwise or counter-clockwise, are charge-dependent. The eight insets in Figure 4 are selected examples of bubble chamber tracks of electrons, positrons, π-mesons and protons in magnetic fields (6-12) and Table 3 lists the derived attenuation coefficients by particle type. In the absence of electron energy loss, Lawrence (13) showed that the theoretical electron trajectory in an H-field is an overlapping circle. Although it is generally acknowledged in the literature that inward spiral tracks are due to energy loss by radiation and collisions, no theoretical model for such a spiral track has been developed. Figures 3 and 4 reveal an astonishing fact; even though the tracks are drawn from different events and bubble chambers, they can all be mathematically interpreted in terms of the simple polar equation for an inward winding spiral:

$$r = r_0\, e^{-\alpha\theta} \qquad\qquad\qquad -(8)-$$

$$\ln r = \ln r_0 - \alpha\theta \qquad\qquad\qquad -(9)-$$

In Equations (8) and (9), $r$ and $r_0$ can be in arbitrary but consistent units, and the polar angle $\theta$ is in radians. The data displayed in Figure 3 was digitized by loading the desired track image into Matlab® and using its *ginput* command to digitize the track by manual mouse clicks at judicious crosshair locations on the track. Since the angular positions are preserved in images, the attenuation factor, $\alpha$, is preserved through undistorted image magnifications. Figure 3 is an example of the fit to Equation (9) of the $K^+$ decay products, from Alvarez (11, Figure 4b, upper right panel).

Equation (8) provides a useful phenomenological reference to an analytical theory for a charged particle track in an H-field. The phenomenological theory for the motions of charged particles in magnetic fields proposed in this paper is based on modeling the radiative energy loss of a particle as being due to a retarding force obeying Lenz's law.
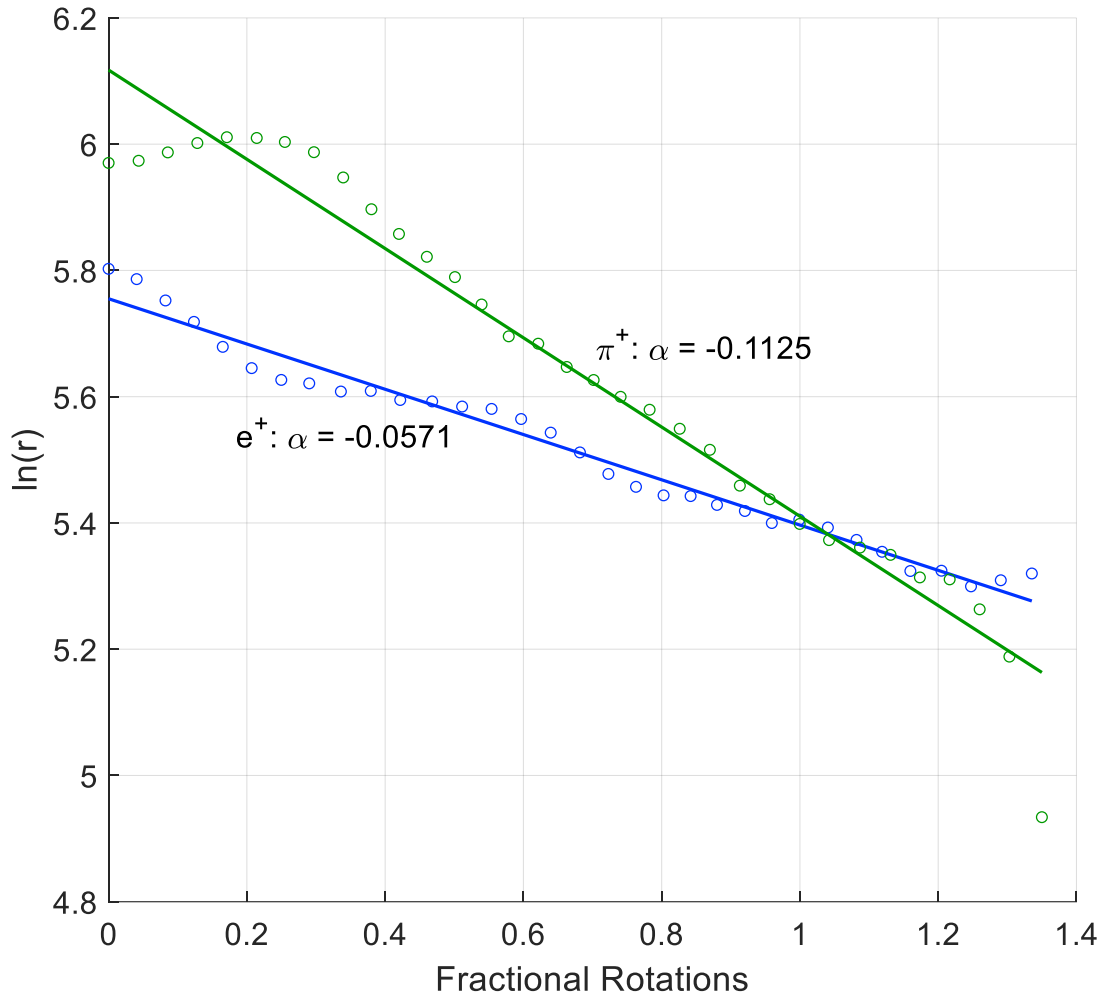
**Figure 3**. *Typical linear least-squares fit of bubble chamber tracks to Equation (9).*
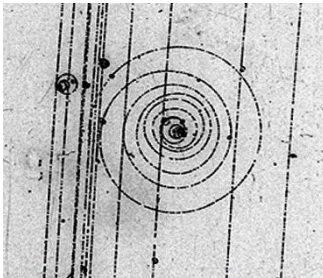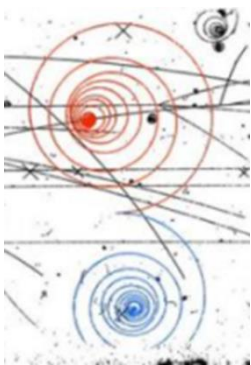
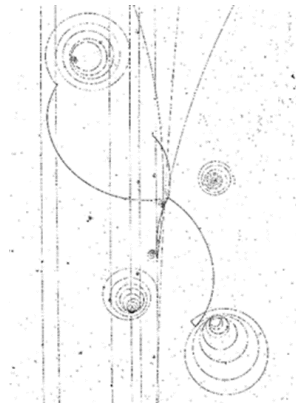| Image & Particles | Reactions & Reference | $\alpha$ | Image & Particles | Reactions & Reference | $\alpha$ |
|---|---|---|---|---|---|
|  | Proton-Anti-proton Annihilation: $$p^+ + p^- \rightarrow 2\pi^+ + 2\pi^- + \pi^0;$$ $\pi^+ \rightarrow \mu^+ + \nu_\mu;$ $\mu^+ \rightarrow e^+ + \nu_\mu;$<br><br>Reference: 6 | $e^-$: 0.0406<br><br>$e^+$: 0.0402<br><br>$\pi^+$: 0.0942 |  | Lone $e^-$, Reference: 7 | $e^-$: 0.0436 |
|  | $e^-, e^+$ Pair Production<br><br>Reference: 8 | $e^-$: 0.0550<br><br>$e^+$: 0.0516 |  | $K^+$ Decay: $K^+ \rightarrow 2\pi^+ + \pi^-;$ $\pi^+ \rightarrow \mu^+ + \nu_\mu;$ $\mu^+ \rightarrow e^+ + \nu_\mu;$<br><br>Reference: 9 | $e^+$: 0.0406<br><br>$e^+$: 0.0314 |

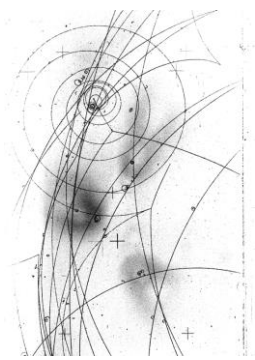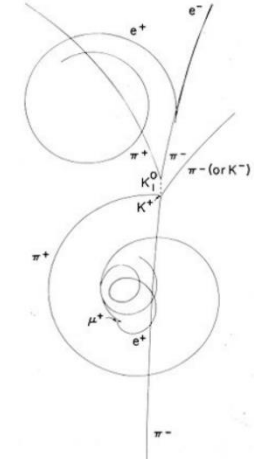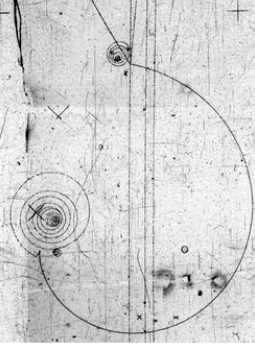**Figure 4a.** *Select bubble chamber track set 1, fitted to the simple spiral equation (9), above.*

| Image & Particles | Reactions & Reference | $\alpha$ | Image & Particles | Reactions & Reference | $\alpha$ |
|---|---|---|---|---|---|
|  | Dalitz pair production in a simple charge exchange reaction:<br>$\pi^+ + n \rightarrow \pi^0 + p^+$;<br>$\pi^0 \rightarrow \gamma + \gamma$;<br>$\gamma \rightarrow e^+ + e^-$<br><br>Reference: 10 | $e^+$: 0.0649 |  | $K^+$ Production & Decay:<br>$\pi^- + p^+ \rightarrow K^+$;<br>$K^+ \rightarrow 2\pi^+ + \pi^-$;<br>$\pi^+ \rightarrow \mu^+ + \nu_\mu$;<br>$\mu^+ \rightarrow e^+ + \nu_\mu$;<br><br>Reference: 11 | $e^+$: 0.0571<br><br>$\pi^+$: 0.1125 |
|  | $\pi^+$ Decay<br><br>$\pi^+ \rightarrow \mu^+ + \nu_\mu$;<br>$\mu^+ \rightarrow e^+ + \nu_\mu$;<br><br>Reference: 12 | $e^+$: 0.0477<br><br>$\pi^+$: 0.1269 |  | $\pi^+$ Decay<br><br>Reference: 8 | $e^+$: 0.1890<br><br>$\pi^+$: 0.1125 |

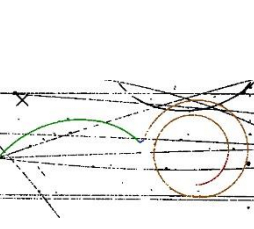**Figure 4b.** *Select bubble chamber track set 2, fitted to the simple spiral equation (9), above.*

**Table 3**. *Attenuation factors, α, for the selected images of Figures 4*

| Image | α $e^-$ | $e^+$ | $\pi^+$ | $p^+$ | Reference |
|---|---|---|---|---|---|
| Fig 4a, upper left | 0.0406 | 0.0402 | 0.0942 | | 6 |
| Fig 4a, upper right | 0.0436 | | | | 7 |
| Fig 4a, lower left | 0.0550 | 0.0516 | | | 8 |
| Fig 4a, lower right | | 0.0406 | | | 9 |
| | | 0.0314 | | | |
| Fig 4b, upper right | | 0.0649 | | 0.0852 | 10 |
| Fig 4b, upper left | | 0.0571 | 0.1125 | | 11 |
| Fig 4b, lower left | | 0.0477 | 0.1269 | | 12 |
| Fig 4b, lower right | | 0.0578 | 0.1890 | | 8 |

The total force on the charged particle in a magnetic field, $\vec{B}$ is then a modification of the Lorentz motive force by adding the modeled radiation damping retarding force:

$$F = e\,\vec{v} \times \vec{B} - e\,\alpha\,\frac{\vec{B} \times \vec{v} \times \vec{B}}{|\vec{B}|} \qquad\qquad -(10)-$$

The vector formulation and sign of the attenuation term in Equation (10) ensure that the attenuating force is in a direction opposite to the forward tangential velocity vector, $\vec{v}$.

Because the first Lorentzian term of Equation (10) describes a radial, centripetal force, and its second damping term describes a retarding tangential damping force, Equation (10) allows an independent solution formulation for each term. For a track in circular motion with tangential velocity of $v$, the Lorentzian term in Equation (10) can be

expressed as:

$$m_e \frac{v^2}{r} = e\,B\,v \qquad\qquad -(10a)-$$

which has the convenient solution given by Lawrence (13) of a constant angular velocity despite a continuously dampened tangential velocity.

$$\omega = \frac{v}{r} = \frac{e\,B}{m_e} \qquad\qquad -(10a)-$$

The constancy of the angular velocity, $\omega$, simplifies the solution for the spiral trajectory characterized by the tangential dampening force, of Equation (10).

$$m_e\,\dot{v} = -\alpha\,e\,B\,v \qquad\qquad -(10b)-$$

$$\frac{\dot{v}}{v} = -\alpha\,\omega \qquad\qquad -(10b)-$$

Equation (10b) is amenable to the simple analytical solution:

$$v = v_0\,e^{-\alpha\,\theta} \qquad\qquad -(11)-$$

where $v_0$ is the track's tangential speed at time $t = 0$. Equation (11) can be reduced to a phenomenological track equation using the continuous polar angle of the track ($\theta = \omega t$) and the angular velocity definition in Equation (10a), $\omega = \frac{v}{r}$:
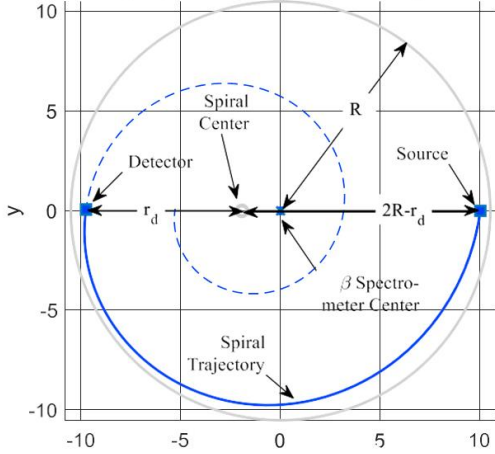
$$r = r_0\,e^{-\alpha\,\theta} \qquad\qquad -(11a)-$$

The simple Lentz formulation for the retarding force on the charged particle is thus seen to lead to the simple intuitive track trajectory that was used previously to fit the bubble chamber track data (Equation 8, Figure 4).

The theoretical spiral trajectories, although tested above with bubble chamber trajectories, can be further validated with experimental data from a selected number of modern laboratory β-spectrometers (or half-turn cyclotrons). The selection of spectrometer datasets to be used for the validation (References 14 to 17) is based on considerations of the simplicity of design, testing and calibration procedures, and the potential accuracy of the measurements.

Figure 5 shows how the spiral trajectory reference center is displaced with respect to the geometric center of the spectrometer. Figure 5 also shows a typical spectrometer design and its main components. Bartlett and Correl (14) use a Bucherer-style velocity selector in front of its detector, while the remaining designs use the spectrometer's magnetic field as the velocity selector together with calibrated solid state kinetic energy detectors.
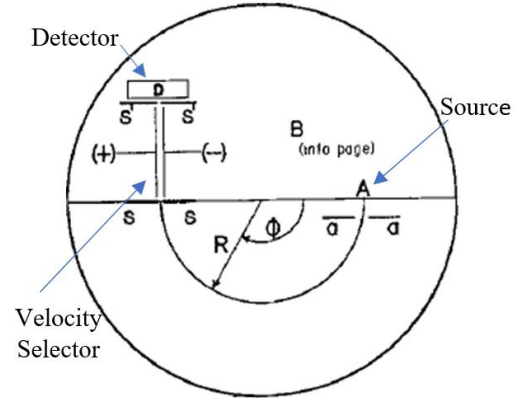
**Figure 5.** *Left panel: Reference spiral trajectory to β spectrometer.*
*Right panel: β spectrometer components (8)*

The procedure used to fit the spectrometer data to the theoretical trajectory of Equation (8 or 11a) is as follows:

1.  Calculate the trajectory's operating angular velocity, $\omega$, from the operating value of the magnetic field.

2.  Deduce the final electron speed ($v_f$) from the measured kinetic energy. Bartlett and Correl (14) report $v_f$ directly.

3.  Apply Equation (10a) to obtain the final radial distance, $r_d = \frac{v_f}{\omega}$, of the electron at the detector to the spiral center

4.  Impose the constant $\omega$ condition to determine the radial distance of the electron at its source to the center of the spiral trajectory (= $2R - r_d$), as shown in Figure 5.

5.  Calculate the initial velocity of the electron at the source, again by imposing constant $\omega$ condition as: $v_i = (2R - r_d)\omega$

6.  Calculate $\alpha$ using Equation (9 or 11) for a final angular position of $\theta = \pi$, as:

$$\alpha = -\frac{1}{\pi} \ln\left(\frac{v_f}{v_i}\right) = -\frac{1}{\pi} \ln\left(\frac{r_d}{2R - r_d}\right)$$
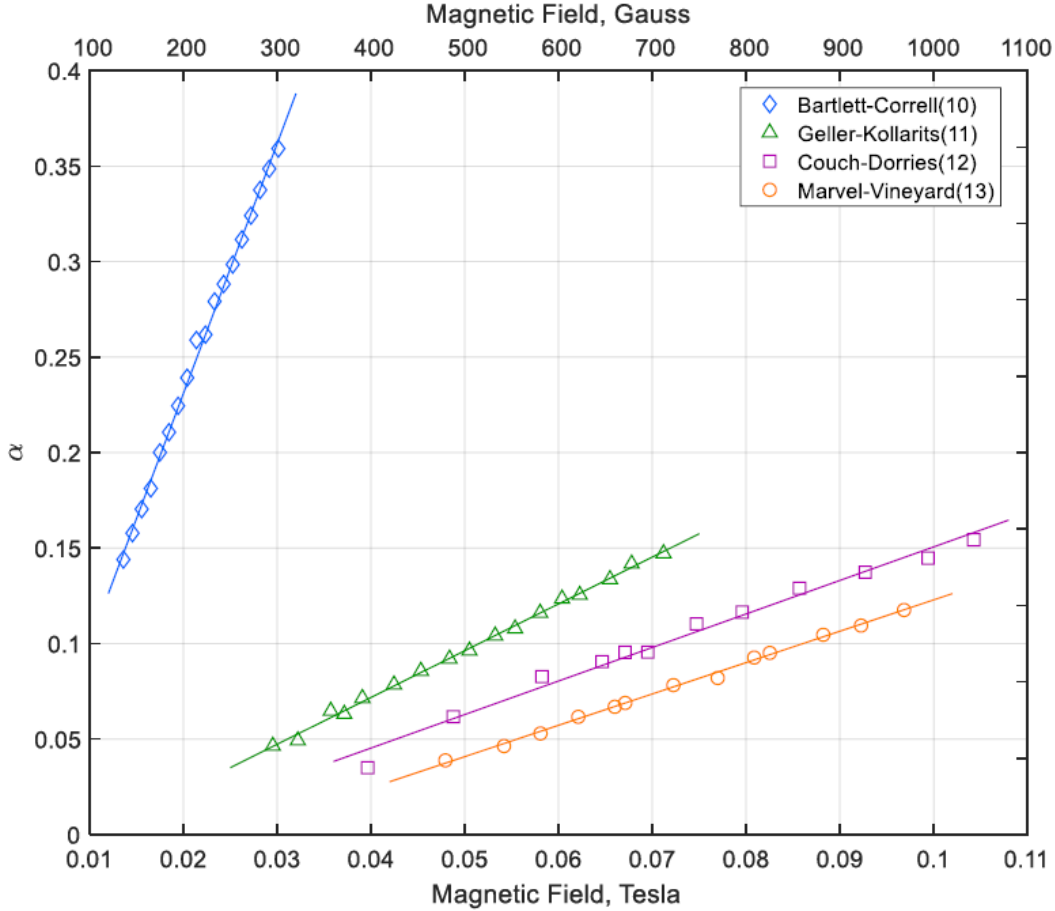
**Figure 6.** *Radiation damping attenuation constants for electrons in a magnetic field from spectrometer measurements.*

Figure (6) summarizes the attenuation coefficients, $\alpha$, obtained as outlined above, from all 4 data sets. Although the simple model for radiation damping presented above leads theoretically to the spiral trajectory solution that appears to fit bubble chamber tracks and the spectrometer data for a unique value of the magnetic field, the damping constant $\alpha$ itself appears to depend on the magnitude of the magnetic field. Table 1's bubble chamber track attenuation coefficients for electrons and positrons appear to be in a range consistent with their potential dependence on magnetic field. Velocity damping occurs both by energy loss by radiation as well as by Bethe-Bloch mechanisms. The close fit of the trajectories to Equation (11a) indicates that both mechanisms are phenomenologically well represented by Equation (10). Hence the present formulation, while phenomenologically useful at a single value of the magnetic field, a constant attenuation coefficient, $\alpha$, does not capture the full radiation or

collisional mechanism satisfactorily. The following characteristics of the $\alpha$ values are evident:

1.  $\alpha$ appears to be dependent linearly on the magnetic field. It's not clear if the above behavior is a result of the simplified, constant $\omega$, solution to Equation 10. In this regard, an evaluation of a full, uncoupled solution to Equation 10 is currently in progress.

2.  The Bartlett and Correll (14) data show $\alpha$ values significantly larger than the remaining 3 data sets that are roughly grouped together.

3.  There appears to be significant experimental error in determining $\alpha$ as judged from their significant deviations among the data sets.

4.  The 3 data sets that are roughly grouped together appear to agree reasonably with the previously discussed $\alpha$ values from bubble chamber trajectories.

The above behaviors can be valuable in further refinements of the spectrometer experiments, and further theoretical understanding of the mechanisms involved in the radiation-induced and collisional damping constant, $\alpha$.

## 2.2 Electron Motion in Electric Fields

In his classic experiment, Bertozzi(18) demonstrated that electrons accelerated by an electric field were speed limited, however high the magnitude of the imposed electric field. Bertozzi invoked SR's universal speed limit to explain the result. However, the measurements of faster-than-light $\mu$-meson flight speeds presented in Section 1 no longer permit the universal speed limit to be a viable explanation. In the previous Section, a new model for the radiation damping of the tangential velocity of electrons in a magnetic field, led to an elegant analytical solution for the observed inward spiral bubble chamber and spectrometer tracks of charged particles in magnetic fields. The proposed new analogous force model for charged particles in electric fields, including the radiation damping Lentz force, is:

$$F_e = m_e \vec{a} = e\vec{E} - \frac{e}{c}(\vec{v} \cdot \vec{E})\frac{\vec{E}}{|\vec{E}|} \qquad -(12)-$$

Equation 12 has no phenomenological constants in comparison with the force formulation in the magnetic field in Equation 10. When applied to the Bertozzi

experiment of the electric field and electron motion limited to the x-direction, Equation (12) becomes:

$$m_e \dot{v} = eE - e\frac{v}{c}E \qquad\qquad -(13)-$$

The solution to Equation (13) for an initial zero electron velocity, is:

$$\beta = \frac{v}{c} = \left(1 - e^{-\frac{t}{\tau_E}}\right),\ \tau_E = \frac{c\, m_e}{eE}, \qquad E = \frac{V}{d} \qquad -(14)-$$

$$x(t) = \int_0^t v(t')\, dt' = ct - c\,\tau_E\left(1 - e^{-\frac{t}{\tau_E}}\right) = ct - v(t)\tau_E \quad -(15)-$$

Subject to the initial condition of $v = 0$ at $t = 0$. In Equations 14 and 15, $\tau_E$ is the characteristic time required to reach the limiting speed of c, and is inversely proportional to the electric field. Equations 14 and 15 are directly applicable to Bertozzi's first three data points obtained with only the van De Graff generator activated and the LINAC disabled. Because the Van de Graff chamber length, d, is not disclosed, it is determined from numerical optimization that minimizes the error between the theoretical predictions and experimental results. Under the above controlled conditions, Equation 15 is first applied to obtain the time of flight for an assumed Van de Graff chamber length, d. Equation 14 is then used to calculate the electron's final velocity out of the E-field-active van de Graff section and into the coasting section.

Figure 6 shows the theoretical time variation of the electron speed and its traversed distance. The asymptotic straight lines of equal slope, indicative of the speed limitation, and intercepts varying with the electric field are evident in the lower panel of Figure 6. The three experimental points form Bertozzi are also marked on the plots. Table 3 summarizes the above comparison.

Table 4 shows that the optimal estimate of 0.8 m for the length of the E-field-active van de Graff section of the Bertozzi experiment leads to excellent prediction of the total time for all cases of E, especially for E = 1.0 and 1.5 million volts. The close agreement shown in Table 1 between predictions and experimental results is a validation of the damping force formulation of Equation (12).
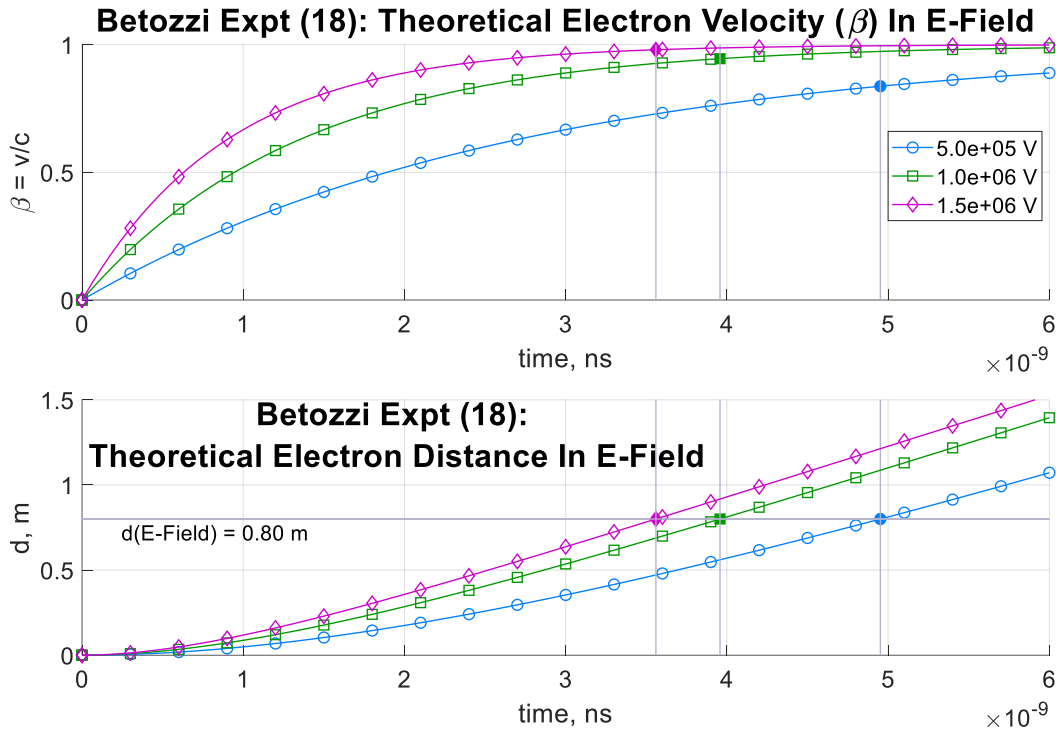
**Figure 6.** *Theoretical electron velocity and distance traversed in the E-field section of Bertozzi's experiment (18).*

**Table 4.** *Theoretical electron velocity, distance traversed and time of traverse in the E-field section of Bertozzi's experiment (18), compared with measurements.*

| Dist in E-Field, m | V, volt | E, V/m | Coast-ing Dist , m | Theor-etical $\frac{v_{final}}{c}$ | Theoretical Electron Travel Times, s | | | Measured Total Time, s | Total Travel Time Error (Theory-Exp), s |
|---|---|---|---|---|---|---|---|---|---|
| | | | | | E-Field | Coast | Total | | |
| | 5.0E+05 | 6.25E+05 | | 0.84 | 4.95E-09 | 3.03E-08 | 3.52E-08 | 3.23E-08 | -2.93E-09 |
| 0.80 | 1.0E+06 | 1.25E+06 | 7.60 | 0.95 | 3.96E-09 | 2.68E-08 | 3.08E-08 | 3.08E-08 | 1.90E-11 |
| | 1.5E+06 | 1.88E+06 | | 0.98 | 3.56E-09 | 2.59E-08 | 2.94E-08 | 2.92E-08 | -2.26E-10 |
| | | | | | | | | RMS Error,s | 1.70E-09 |

# 3. Transverse Doppler Effect

The remarkable experiments of Ives and Stillwell (19, 20) and Kundig (23) perhaps provide the most compelling evidence in favor of the relativistic transverse doppler effect, which is classically forbidden. Figure 7 summarizes the data from the experiments by Ives and Stillwell and Kundig fitted to the relativistic prediction:

$$\frac{\Delta E_\nu}{E_\nu} = \frac{1}{2}\left(\frac{v}{c}\right)^2 = \frac{1}{2}\beta^2 \qquad\qquad -(16)-$$
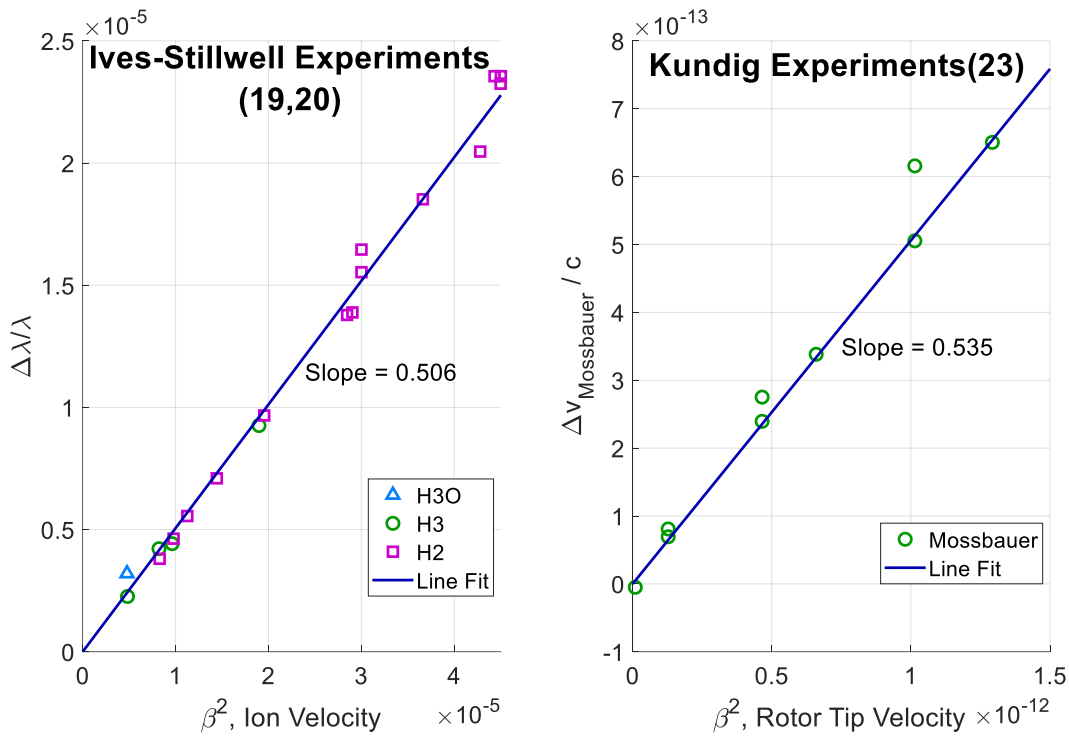


**Figure 7.** *Analyses of the data from the experiments of Ives and Stillwell (19, 20), left panel, and of Kundig (23), right panel, to the relativistic theory:* $\frac{\Delta E_\nu}{E_\nu} = \frac{1}{2}\beta^2$

In the above figure, it is astonishing that both experiments, despite their widely different experimental conditions, closely conform to the SR-predicted ½ slope, a compelling observation that points to an inherent common truth in the two different

phenomena captured by the two experiments. In the Ives & Stillwell experiments, it is not clear if the observed second-order shifts are attributable exclusively to a transverse Doppler effect, since the observation of the smaller second-order shifts is only possible by receiving the light in the transverse direction to filter out the larger standard Doppler shifts. It is possible that the second-order shifts are distributed in all directions by collisions but are only measurable in the transverse direction. In the Kundig experiment, the gamma rays are not subjected to acceleration in flight from the source, but only in the infinitesimally short time it is captured in the detector. The theoretical justification for a transverse Doppler effect is tenuous in the Kundig experiment as well. A single feature common to both experiments is that the energy shifts are observed in accelerated photon emitters or photon absorbers. In the Ives & Stillwell experiment, the photons were emitted from accelerated ions, whereas in the Kundig experiment, the $\Upsilon$ photons were subject to the centripetal acceleration when absorbed in the receive detector.

The classical explanation offered here is that the above second order shifts are due to impulsive momentum transfer, $\Delta p_v$, to a photon when it is emitted or absorbed from an accelerating source or receiver. In the Ives & Stillwell experiment the visible light energy emitted by the acceleration ions are blue shifted, whereas in the Kundig experiment, the gamma photons are red shifted as they are impulsively absorbed into the receiver. In both cases, the impulsive momentum transfer is:

$$\Delta p_v = \frac{\Delta E_v}{c} = F_v \, \Delta t_v \qquad\qquad - (17) -$$

where $F_v$ is the impulse force on the photon, and $\Delta t_v$ is the action time of the impulse force on the photon.

## 3.1 Ives-Stillwell (IS) Experiment

Ives and Stillwell observed the transverse Doppler shifts in accelerated canal rays ($H_2$, and $H_3$ ions) emitting the second line of the Balmer series (H$\beta$ line, $\lambda$=4861 $A^o$; the $H_3O$ line is $\lambda$= 3749 $A^o$). Equation (17) can be adapted for the IS experiment, as follows:

$$\frac{\Delta E_v}{c} = F_v \, \Delta t_v = m_v \frac{eE}{M_m} \Delta t_v = m_v \frac{eV}{dM_m} \Delta t_v = \frac{E_v}{c^2} \frac{eV}{dM_m} \Delta t_v = \frac{1}{2} \frac{E_v}{c^2} \frac{v^2}{d} \Delta t_v \qquad - (18) -$$

$$\Delta p_v = \frac{\Delta E_v}{c} \qquad\qquad - (19) -$$

$$eV = \frac{1}{2} M_m v^2 \qquad\qquad - (20) -$$

$$m_v = \frac{E_v}{c^2} \qquad\qquad -(21)-$$

where:

$\Delta E_v$ = the photon energy shift

$c$ = the speed of light

$F_v$ = the impulse force on the photon

$\Delta t_v$ = the duration of the impulse force

$m_v$ = the effective mass of the photon

$M_m$ = the mass of the photon-emitting ion

$v$ = the ion velocity

$e$ = the electron charge

$E$ = the electric field accelerating the photon-emitting molecules

$V$ = the ground-referenced voltage between the acceleration parallel plates

$d$ = the spacing between the acceleration parallel plates

$\tau$ = the lifetime of the photon emitter or absorber

A simplified form, experimentally verifiable form of Equation (18), is:

$$\frac{\Delta E_v}{E_v} = \frac{1}{2}\frac{v^2}{c^2}\frac{\Delta t_v}{\left(\frac{d}{c}\right)} \qquad\qquad -(22)-$$

where $\Delta t_v$ is the time of the impulsive force on the photon. The experimental result of Equation (16) leads to the constraint that:

$$\frac{\Delta t_v}{\left(\frac{d}{c}\right)} = 1, \qquad \Delta t_v = \frac{d}{c} = \left[\frac{\left(\frac{d}{c}\right)}{\tau}\right]\tau = f\tau, \qquad f = \left[\frac{\left(\frac{d}{c}\right)}{\tau}\right] \qquad -(23)-$$

Because the emitted photon is in formed within the emitting ion as the ion is accelerated, it would be reasonable to expect that $\Delta t_v$ is the lifetime of the excited state of the emitting ions, which Dempster (21, 22) had estimated to be about $3\times10^{-10}$ sec. However, the $\frac{d}{c}$ term for the IS experiment was about $5\times10^{-12}$ sec. It was originally thought that the photon first behaves as a particle in its impulse momentum transfer,

and then as a wave when the impulse transfer is subsequently detected as a wavelength or frequency shift.  However, the experimentally observed ½ slope indicates that the impulsive momentum transfer process is far more complex than the initial perception, with the characteristic time of light traversing the acceleration distance determining the fraction of the impulsive momentum transferred.

## 3.2 Kundig Experiment

In the Kundig experiment, the impulsive force on the photon is centripetal. Hence the equivalent of Equation (17) for the Kundig's Mossbauer experiment is:

$$\frac{\Delta E_v}{c} = m_v r \omega^2 \Delta t_v = m_v \frac{v^2}{r} \Delta t_v = \frac{E_v}{c^2} \frac{v^2}{r} \Delta t_v \qquad - (24) -$$

$$\frac{\Delta E_v}{E_v} = \frac{v^2}{c^2} \frac{\Delta t_v}{\left(\frac{r}{c}\right)} \qquad - (25) -$$

where:
$r$ = the rotor radius
$\omega$ = the rotor angular speed
$v = r\,\omega$, the rotor tip speed

As in the IS experiment, the experimental result of the slope of ½ requires for Equation (25):

$$\frac{\Delta t_v}{\left(\frac{r}{c}\right)} = \frac{1}{2}, \qquad \Delta t_v = \frac{1}{2}\left(\frac{r}{c}\right) = f\tau, \quad f = \frac{1}{2}\frac{\left(\frac{r}{c}\right)}{\tau} \qquad - (26) -$$

In the Kundig experiment, the Mossbauer absorption nucleus has a well-defined lifetime of $10^{-7}$ sec which is much larger than $\left(\frac{r}{c}\right) = 3\text{x}10^{-10}$ s.  As in the IS experiment, the impulse time, $\Delta t_v$, appears to be a fraction of the full impulse time, $\tau$, the lifetime of the absorbing nucleus, determined by a photon's characteristic time of flight in the experiment.  The factor of ½ in Equation (26) is difficult to justify, since the Ives & Stillwell experiment infers an impulse time proportional to the photon flight time without a fraction of ½.

# 4. Analysis Of Special Relativity's Time Dilation Formulation

## 4.1 Rotational Ambiguity Of Time Dilation (Contraction) Formulation

The SR time-dilation formulation is not invariant with respect to the rotation of the light clock. The appearance of a light clock inclined at angle $\varphi$ in the moving frame to the fixed frame observer is shown in Figure 8. In this case, the clock period in the fixed frame appears dilated for the light clock upstroke and contracted for the light clock downstroke, as explained below. If the clock period in the rest frame is, $t_0$, SR's upstroke clock period in the moving frame, $t_{1u}$, is given by:
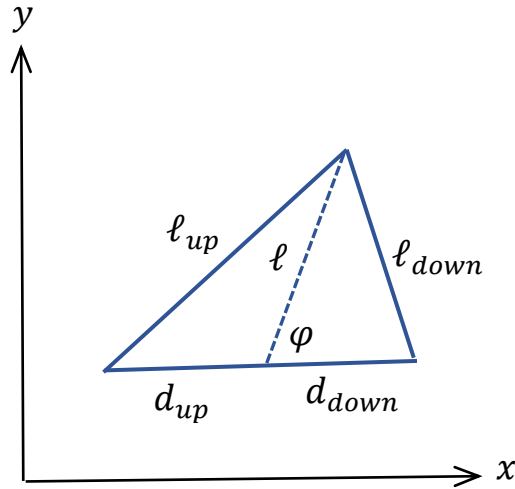


**Figure 8.** *Rest frame observation of the up and down strokes of a moving light clock inclined at angle $\varphi$.*

$$d_{up} = v\, t_{up} \qquad\qquad -(28)-$$

$$\ell_{up} = c\, t_{up} \qquad\qquad -(29)-$$

$$\ell = c\, t_0 \qquad\qquad -(30)-$$

$$\ell_{up}^2 = \ell^2 + d_{up}^2 + 2\ell d_{up} \cos\varphi \qquad\qquad -(31)-$$

$$c^2 t_{up}^2 = c^2 t_0^2 + v^2 t_{up}^2 + 2cv t_0 t_{up} \cos\varphi \qquad\qquad -(32)-$$

$$\left(1 - \frac{v^2}{c^2}\right) t_{up}^2 - 2\frac{v}{c} t_0 t_{up} \cos\varphi - t_0^2 = 0 \qquad -(33)-$$

$$t_{up} = \frac{\beta \cos\varphi + \sqrt{\beta^2 \cos^2\varphi + \gamma}}{\gamma} t_0 \ , \beta = \frac{v}{c} \ , \gamma = 1 - \frac{v^2}{c^2} \qquad -(34)-$$

$$t_{dn} = \frac{-\beta \cos\varphi + \sqrt{\beta^2 \cos^2\varphi + \gamma}}{\gamma} t_0 \qquad -(35)-$$

Equations (28) to (30) are distances observed in the fixed frame for the upstroke clock period, and Equation (31) is the trigonometric distance constraint of the upstroke triangle of Figure (8). Equation (32) is derived by combining Equation (31) with Equations (28) to (30). For the inclined clock, the time-dilated upstroke clock period in the fixed frame is given by the quadratic equation of Equation (33), and Equation (34) is its positive solution. In the same manner, the contracted period of the light clock in the downstroke, as observed in the fixed frame, is given by Equation (35). Figure (8) verifies that for the inclined clock, for inclination angles:

$0 < \varphi < \frac{\pi}{2}$, because , $d_{up} > \ell$ and $d_{dn} < \ell$ , the light clock is dilated in the upstroke and contracted in the downstroke. The opposite holds for the inclination-angle range: $\frac{\pi}{2} < \varphi < \pi$, when the clock is contracted in the upstroke dilated in the downstroke. It is only in the special case of $\varphi = \frac{\pi}{2}$ considered in SR that the clock is dilated in both the upstroke and downstroke.

SR's assertion of time dilation is only true for a special case of a clock orientation of $\varphi = \frac{\pi}{2}$. The light clock's general dependence on the inclination of the light clock, and the clock stroke, causes the time dilation formulation to predict a confusion of unworkable ambiguities, especially because SR provides no guidance as to the selection of the light clock's orientation. In addition, μ-mesons arrive from all directions, and it is not at all clear how a singly oriented light clock can generally apply to μ-mesons arriving from all directions. Furthermore, the speed of sound at a fixed temperature and pressure is a constant across all inertial frames and can be implemented in hermetically sealed cartridges. SR's time dilation formulation is additionally ambiguous with respect to the clock type, that is light vs. sonar.

Thus, SR's time dilation concept is unacceptable because it is not invariant to its clock orientation or to the clock type.

## 4.2 Alternate Time Dilation Formulation By Galilean Velocity Transformation

Newton's inertial frame of reference includes both the observer and apparatus. In a modified thought experiment that adds an identical clock to the fixed frame and an observer to the moving frame, observers in both frames would measure exactly the same clock period in accordance with C5, and the time dilation issue would never have arisen. SR's time dilation formulation arises simply from the separation of observer and apparatus. In this case, the relative speeds of the up and down clock strokes observed in the fixed frame cannot be expected to be c, since C5 is no longer applicable. Rather, the ray motion of the moving clock must be translated to the fixed frame by a Galilean velocity transformation. Figure (8) shows that the Galilean velocity of the light clock ray in the upstroke as observed in the fixed frame is not c, but is given by:

$$\vec{v}_{up} = \vec{v} + \vec{c} \qquad\qquad -(36)-$$

With magnitude, $v_{up}$, given by (Referencing Figure (8)):

$$v_{up}^2 = c^2 + v^2 + 2cv \cos\varphi \qquad\qquad -(37)-$$

The fixed frame and moving frame clock periods are now related by Equation (32), but with the speed of the clock ray observed in the fixed frame c, in the original SR formulation on the left-hand side, replaced by $v_{up}$, as given by Equation (37):

$$v_{up}^2 t_{up}^2 = c^2 t_0^2 + v^2 t_{up}^2 + 2cvt_0 t_{up} \cos\varphi \qquad\qquad -(32/38)-$$

Substituting for $v_{up}$ from Equation (37) transforms Equation (38), as:

$$t_{up}\left(c^2 t_{up} + 2cv\, t_{up}\cos\varphi\right) = t_0\left(c^2 t_0 + 2cvt_{up}\cos\varphi\right)$$

with the profound solution of time invariance in the two frames:

$$t_{up} = t_0 \qquad\qquad -(39)-$$

Hence, the application of Galilean velocity transformation to SR's virtuial experiment indicates no time dilation, in full accordance with C5. The absence of time dilation resolves the issue of ambiguities, because every light clock orientation yields the same clock period for the observer at rest as in the moving frame.

# Discussion

SR arose from the need for a theoretical justification for the null result of the Michelson-Morley (MM) experiment. The time-dilation formulation, derived purely from an analysis of a virtual experiment, is widely accepted without the essential rigorousness checks discussed in this paper. However, time dilation alone could not explain the MM result. It was then theorized that simultaneous space contraction (Lorentz-Fitzgerald contraction) maintains the constancy of the speed of light. Hence the space-time Lorentz transformation, and its generalization in the modern covariance theory, are traceable to SR's time dilation result. If time dilation is not valid, both the Lorentz transformation and the covariance theory are invalid.

This paper has shown that SR is foundationally untenable, and that Newton's laws alone are sufficient to simply and stylishly explain the major experiments believed to support SR. New remarkable discoveries have resulted from the current Newtonian pursuit:

(1) Upper-atmospheric μ-mesons travel at speeds exceeding the speed of light

(2) A simple model for radiation damping explains the experimentally measured tracks of charged particles subject to electric and magnetic fields

(3) A new impulsive momentum transfer phenomenon appears to explain experimental results which are believed to support a transverse Doppler effect. The impulsive momentum phenomenon joins the Compton effect, and electro-proton annihilation as processes in which the wave-particle duality of light is experimentally manifested.

However, the explanations provided in this study are incomplete. The dependence of the attenuation coefficient on the magnitude of the applied magnetic field needs to be explained. Also, the discovery that the impulsive momentum transfer times are driven by characteristic light transit times and not by the lifetimes of the photon emitters is unexpected and needs further investigation.

This study is just a starting point. Much work needs to be done to verify the applicability of Newton's laws to fundamental particle kinematics.

# Conclusion

New fundamental realizations emerge from this paper:

(1)  No universal upper speed limit
(2)  Constant mass across inertial frames (no need to for the term "rest mass")
(3)  Constant time differences across inertial frames (no perceived time dilations)
(4)  The kinetic energy of a particle is simply $\frac{1}{2}mv^2$ (no relativistic total energy)
(5)  Restoration of the validity of the kinetic energy theorem
(6)  Inclusion of the radiation damping force is essential for explaining the motion of charged particles in electric and magnetic fields
(7)  No transverse Doppler effect
(8)  Impulsive momentum transfer is a viable new phenomenon.

It is hoped that this paper will catalyze a new discourse on their validations and their impact on the future progression of physics.

# References

1. Newton, I. Philosophiae Naturalis Principia Mathematica, Streater, London (1687)
   Newton, I. Principles of Natural Philosophy, Univ of California Press, Berkeley, (1934); paperback, (1962)

2. Einstein, A. Zur Elektrodynamik bewegter Körper, *Ann. der Physik 17, 891 (1905)*

3. Rossi, B., Sands, M., and Sard, R. F., Measurement of the Slow Meson Intensity at Several Altitudes, *Phys. Rev., 72 (2), 120 (1947).*

4. Rossi, B., and Hall, D. B., Variation of the Rate of Decay of Mesotrons with Momentum, *Phys. Rev., 59 (3), 223 (1941).*

5. Rossi, B., Hillbery, N., and Hoag, J. B., The Variation of the Hard Component of CosmicRays with Height and the Disintegration of Mesotrons, *Phys. Rev., 57 (6), 461 (1940).*

6. University of California, Berkeley bubble chamber photograph, U.S. National Archives & DVIDS, Public Domain Archive
   https://nara.getarchive.net/media/bubble-chamber-event-resonances-last-typically-for-a-mere-10-23-power-seconds-9a8ba1

7. CERN bubble chamber image archive:
   http://hst-archive.web.cern.ch/archiv/HST2005/bubble_chambers/BCwebsite/index.htm
   (electron)

8. Woithe, J., Schmidt, R. and Naumann, F., *Track inspection: how to spot subatomic particles*, CERN S'Cool LAB website:
   https://scoollab.web.cern.ch/bubble-chamber-pictures-classroom

9. CERN bubble chamber image archive:
   http://hst-archive.web.cern.ch/archiv/hst2005/bubble_chambers/bcwebsite/gallery/gal2_11.htm

10. CERN bubble chamber image archive: http://hst-archive.web.cern.ch/archiv/hst2005/bubble_chambers/bcwebsite/gallery/gal2_20.htm

11. Alvarez, L. image archive: https://www.visionlearning.com/en/library/Inside-Science/58/Luis-Walter-Alvarez/229

12. CERN bubble chamber image archive: https://hst-archive.web.cern.ch/archiv/HST2005/bubble_chambers/BCwebsite/gallery/gal2_13.htm

13. Lawrence, E. O. and Livingston, M. S. , The Production of High Speed Light Ions Without the Use of High Voltages, *Phys. Rev. 40 (1): 19–35 (1932)* .

14. Bartlett, A. and Correll, M. An Undergraduate Laboratory Apparatus for Measuring as a Function of Velocity. I, *Am. J. Phys. 33, 327 (1965).*

15. Geller. K.N. and Kollarits, R., Experiment to Measure the Increase in Electron Mass with Velocity, *Am. J. Phys. 40, 1125 (1972).*

16. Couch, J. G. and Dorries, T.K. Measuring relativistic electrons in the undergraduate laboratory, *Am. J. Phys. 50, 917 (1982).*

17. Marvel, R. E. and Vineyard, M. F., Relativistic Electron Experiment for the Undergraduate Laboratory, *arXiv:1108.5977v1, (2011).*

18. Bertozzi, W., Speed and Kinetic Energy of Relativistic Electrons, Am. J. Phys. 32, 551 (1964), *Am. J. Phys. 32, 551 (1964).*

19. Ives, E. I. and Stillwell, G. R., An Experimental Study of the Rate of a Moving Atomic Clock, *J. Opt. Soc. Am., 28 (7), 215 (1938).*

20. Ives, E. I. and Stillwell, G. R., An Experimental Study of the Rate of a Moving Atomic Clock. II, *J. Opt. Soc. Am., 31, 369, (1941).*

21. Batho, H. F. and Dempster, A. J., Doppler Effects In Hydrogen Canal Rays Of Uniform Energies, *Astrophys. J., 75, 34 (1932).*

22. Dempster, A. J., The Duration Of The Process Of Light Emission In Hydrogen, *Astrophys. J. 57(4), 193 (1923).*

23. Kundig, W., Measurement of the Transverse Doppler Effect in an Accelerated System, *Phys. Rev., 129(6), 2371 (1963).*